Analysis of functionally graded plates based on a variable separation method

P. Vidal, L. Gallimard, O. Polit, E. Valot

P. Vidal, L. Gallimard, O. Polit & E. Valot (2021) Analysis of functionally graded plates based on a variable separation method, *Mechanics of Advanced Materials and Structures*
DOI: 10.1080/15376494.2021.1942597

Abstract

This work deals with the modeling of plate structures constituted of Functionally Graded Material through a variable separation approach. The displacement field is approximated as a sum of separated functions of the in-plane coordinates x, y and the transverse coordinate z. This choice yields to a non-linear problem that can be solved by an iterative process. Two 2D and 1D linear problems are solved successively. In the thickness direction, a fourth-order expansion in each layer is considered. For the in-plane description, classical Finite Element method is used. The number of unknowns is reduced compared to classical layerwise approach.

Classical numerical tests encountered in the literature are provided to show the accuracy of the present LayerWise (LW) method. The plate can be constituted of a FGM layer or combined FGM/orthotropic layers. Different slenderness ratios and anisotropy indexes are also considered. Accurate results with a low computational cost are obtained when compared with reference solutions and models available in literature.

Keywords: Functionally graded materials, Layerwise approach, Separation of variables, Finite Element

1. Introduction

In this study, Functionally Graded Materials (FGM) in which the mechanical properties vary smoothly and continuously from one surface to the other are considered. To obtain

that, different ways of manufacturing process can be performed (see [1, 2]). One of the advantages is the elimination of the transverse stresses discontinuity which can be encountered in laminated composite. Thus, it allow us to avoid one of the most critical failure mode, i.e. the delamination process. Other attractive characteristics can be mentionned such as: enhanced thermal properties, higher fracture toughness, ... [3]. Note that FGM can be used for a wide field of applications (see [4, 2]). That justifies the increasing interest for this type of materials. Thus, it will be important to have efficient numerical tools so as to compute accurate displacements and stresses for design purpose.

These topics have been the focus of attention of many researchers during the past few years. Different three-dimensional models have been carried out in [5–7] for FGM and sandwich plates, but the computational cost becomes high. Thus, a wide range of 2D models with a low number of generalized unknowns has been developed. For that, the displacements are expressed through the whole thickness of the plate (Equivalent Single Layer model - ESL). Classical Laminate Theory and First-order Shear Deformation Theory (FSDT) have been considered in [8] and [9], respectively. But, the first one fails to predict accurate results for thick cases and the second one needs a shear correction factor. So, Higher-order Shear Deformation Theory (HSDT) has been proposed considering different types of shear strain shape functions: polynomial [10, 9, 11, 12], trigonometric [12], inverse trigonometric [13], specified [14, 15] forms. But, as it has been highlighted in [16], the stretching effect is of major importance for the modeling of this type de materials. Thus, these HSDT models have been extended to take into account this phenomenon. They can be again classified depending of the strain shape functions as previously: polynomial [17–19], trigonometric [20–24], exponential [25], hyperbolic [26, 27], hybrid [22, 25] forms. Note that most of these approaches are built such that the free boundary conditions on the top and bottom surfaces are fullfiled. It should be also mentioned that some of these works needs the determination of one or two parameters involved in the expression of the kinematics, see [23, 27, 13, 12, 15]. This type of models can be well-suited for monolayered structure, but limitations appear considering multi-layered or sandwich panels. An alternative and simple way consists in including the so-called Murakami's zig-zag function as in [18], but more precised theories have

been developed based on a LayerWise approach (LW). Note the extensive works based on the systematic approach developed by Carrera with his Carrera's Unified Formulation (CUF) and its extension to FGM material in [28]. Displacement-based and Reissner's Mixed Variational Theorem (RMVT) approaches are addressed in [29, 16]. Discrete layers have been also considered in [30]. Only partial works on the modeling of FGM plate structures have been given herein and interested readers can refer to the reviews provided in [31, 32, 4, 33, 34].

Over the past years, some methods based on the separation of variables have shown interesting features to model composite structures. For FGM material, the extended Kantorovich method has been applied in [35]. Another interesting way is based on the so-called Proper Generalized Decomposition (PGD). It has been successfully developed for the modeling of laminated and sandwich structures [36–39] and will be extended hereafter for the analysis of FGM plates. In this purpose, the displacements are written under the form of a sum of products of bidimensional functions of (x,y) and unidimensional functions of z. A piecewise fourth-order Lagrange polynomial of z is chosen and a 2D eight-node quadrilateral FE is employed for the in-plane coordinates. Each unknown function of (x,y) is classically approximated using one degree of freedom (dof) per node of the mesh and the LW unknown functions of z are global for the whole plate. Finally, the deduced non-linear problem implies the resolution of 2D and 1D problems alternatively, in which the number of unknowns is smaller than a classical Layerwise approach. Considering the models developed in open literature, it calls for a well-suited kinematics, i.e. a relevant shear strain shape function. The present work allows us to determine automatically the z-functions. Moreover, any configurations could be considered, namely structures constituted of only FGM or combined FGM/classical (laminated) layers.

The article is organized as follows. Firstly, the classical mechanical problem involving a FGM is given. Then, the formulation of the PGD is described in this particular framework. The assumption on the displacements yields a non-linear problem that is solved using an iterative process. The FE discretization is also described. The separation variables can

be efficiently applied as the in-plane and out-of-plane integrations can be split. Finally, numerical results are provided to assess the accuracy of the method. Classical examples are addressed and the results are compared with both reference solutions and results available in open literature. The influence of the slenderness ratio and a characteristic parameter of the FGM (volume fraction exponent) is studied. The present approach also allows us to modelize the FGM with piecewise constant mechanical properties through the thickness at a low computational cost.

2. Reference problem description: the governing equations

Let us consider a composite plate structure occupying the domain $\mathcal{V} = \Omega \times \Omega_z$ where $\Omega = [0, a] \times [0, b]$ (a, b being the dimensions of the plate) and $\Omega_z = [-\frac{h}{2}, \frac{h}{2}]$ in a Cartesian coordinate (x, y, z). h is the thickness of the plate, see Fig. 1.

[Figure 1 about here.]

2.1. Constitutive relation

As we are interested in the analysis of FGM plates, the continuous variations of the material characteristics along the thickness have to be well described. The FGM layers can be single or embedded in other isotropic/orthotropic/FGM layers. Classically, exponential and/or polynomial functions are applied to either engineering constants (Young Modulus, shear Modulus, Poisson ratio) or directly to material stiffnesses C_{ij}.
The plate can be made of NC perfectly bonded classical/FGM layers. The constitutive equations for a layer k can be written as

$$\boldsymbol{\sigma}^{(k)} = \mathbf{C}^{(k)}(z)\boldsymbol{\varepsilon} \quad z \epsilon \Omega_z^k \text{ with } \Omega_z = \cup_{k=1}^{NC} \Omega_z^k \tag{1}$$

where we denote the stress vector by $\boldsymbol{\sigma}$, the strain vector via $\boldsymbol{\varepsilon}$.

We have

$$\mathbf{C}^{(k)}(z) = \begin{bmatrix} C_{11}^{(k)} & C_{12}^{(k)} & C_{13}^{(k)} & 0 & 0 & C_{16}^{(k)} \\ & C_{22}^{(k)} & C_{23}^{(k)} & 0 & 0 & C_{26}^{(k)} \\ & & C_{33}^{(k)} & 0 & 0 & C_{36}^{(k)} \\ & & & C_{44}^{(k)} & C_{45}^{(k)} & 0 \\ & sym & & & C_{55}^{(k)} & 0 \\ & & & & & C_{66}^{(k)} \end{bmatrix} \tag{2}$$

where $C_{ij}^{(k)}$ are the three-dimensional stiffness coefficients of the layer (k).

In the present work, without loss of generality, we assume that we can write the constitutive law as

$$\mathbf{C}^{(k)}(z) = g^{(k)}(z)\ \mathbf{C}_0^{(k)} \tag{3}$$

where $\mathbf{C}_0^{(k)}$ is constant in each layer. If needed, the decomposition of the matrix $\mathbf{C}^{(k)}(z)$ can be splited into several terms to keep the efficiency of the method.
Note that $g^{(k)}(z)$ is constant for a classical isotropic or orthotropic layer.

2.2. The weak form of the boundary value problem

In the present work, a static problem is studied. For conciseness reason, the body force density is not considered. The surface force $\mathbf{t}$ is applied on $\partial\mathcal{V}_F = \partial\mathcal{V}_{F_{xy}} \times \{z_F\}$. We assume that a prescribed displacement $\mathbf{u} = 0$ is imposed on Γ_D. Thus, the classical problem to be solved can be formulated as follows:

Using the above matrix notations and for admissible displacement $\delta\mathbf{u} \in \delta U$, the variational principle is given by:

find $\mathbf{u} \in U$ such that

$$-\int_{\mathcal{V}} \boldsymbol{\varepsilon}(\delta\mathbf{u})^T\, \boldsymbol{\sigma}\, d\mathcal{V} + \int_{\partial\mathcal{V}_F} \delta\mathbf{u}^T \mathbf{t}\, d\partial\mathcal{V} = 0, \qquad \forall \delta\mathbf{u} \in \delta U \tag{4}$$

where U is the space of admissible displacements, i.e. $U = \{\mathbf{u} \in (H^1(\mathcal{V}))^3 / \mathbf{u} = \mathbf{0} \text{ on } \Gamma_D\}$. We have also $\delta U = \{\mathbf{u} \in (H^1(\mathcal{V}))^3 / \mathbf{u} = 0 \quad \text{on} \quad \Gamma_D\}$.

This problem can be expressed as

$$a(\mathbf{u}, \delta\mathbf{u}) = b(\delta\mathbf{u}) \; \forall \delta\mathbf{u} \in \delta\mathcal{U} \tag{5}$$

with

$$\begin{aligned} a(\mathbf{u}, \delta\mathbf{u}) &= \int_{\mathcal{V}} \boldsymbol{\varepsilon}(\delta\mathbf{u})^T \mathbf{C}(z) \boldsymbol{\varepsilon}(\mathbf{u}) \, d\Omega \, d\Omega_z \\ b(\delta\mathbf{u}) &= \int_{\partial\mathcal{V}_F} \delta\mathbf{u}^T \mathbf{t} \, d\partial\mathcal{V} \end{aligned} \tag{6}$$

3. Application of the separated representation to the FGM plate

The present section focuses on the procedure that allows us to expand the PGD to the analysis of FGM layers. This specific separation has shown interesting features in the framework of static analysis [37, 39]. The separated formulation is briefly introduced in the subsequent sections.

3.1. The displacement and the strain field

In the framework of the PGD, the displacement solution $\mathbf{u}$ is classically written as the sum of N products of separated functions ($N \in \mathbb{N}^+$ is the order of the representation)

$$\mathbf{u}(x, y, z) \;\; = \;\; \sum_{i=1}^{N} \mathbf{f^i}(z) \circ \mathbf{v}^i(x, y) \tag{7}$$

where $\mathbf{f^i}(z)$ and $\mathbf{v}^i(x, y)$ are unknown functions which must be computed during the resolution process. $\mathbf{f^i}(z)$ and $\mathbf{v}^i(x, y)$ are defined on Ω_z and Ω respectively. The "$\circ$" operator in Eq. (7) is Hadamard's element-wise product. We have:

$$\mathbf{f}^i \circ \mathbf{v}^i = \mathbf{v}^i \circ \mathbf{f}^i = \begin{bmatrix} f_1^i(z) v_1^i(x, y) \\ f_2^i(z) v_2^i(x, y) \\ f_3^i(z) v_3^i(x, y) \end{bmatrix} \quad \text{with } \mathbf{v}^i = \begin{bmatrix} v_1^i(x, y) \\ v_2^i(x, y) \\ v_3^i(x, y) \end{bmatrix} \; \mathbf{f}^i = \begin{bmatrix} f_1^i(z) \\ f_2^i(z) \\ f_3^i(z) \end{bmatrix} \tag{8}$$

The strain can be expressed with respect to the reference frame in which the dependance with respect to the space coordinates is omitted as follows:

$$\boldsymbol{\varepsilon}(u) = \sum_{i=1}^{N} \begin{bmatrix} f_1^i \, v_{1,1}^i \\ f_2^i \, v_{2,2}^i \\ (f_3^i)' \, v_3^i \\ (f_2^i)' \, v_2^i + f_3^i \, v_{3,2}^i \\ (f_1^i)' \, v_1^i + f_3^i \, v_{3,1}^i \\ f_1^i \, v_{1,2}^i + f_2^i \, v_{2,1}^i \end{bmatrix} \tag{9}$$

where the prime stands for the classical derivative ($f_i' = \dfrac{df_i}{dx}$), and $()_{,\alpha}$ for the partial derivative.

3.2. Formulation of the problem to be solved

An iterative procedure is performed to solve Eq. (5) (greedy algorithm). If we assume that the first n functions have been already computed, the trial function for the iteration $n+1$ is written as

$$\mathbf{u}^{n+1} = \mathbf{u}^n + \mathbf{f} \circ \mathbf{v} = \mathbf{u}^n + \begin{bmatrix} f_1 v_1 \\ f_2 v_2 \\ f_3 v_3 \end{bmatrix} \tag{10}$$

where (f_1, f_2, f_3) and (v_1, v_2, v_3) are the functions to be computed and $\mathbf{u}^n$ is the associated known set at iteration n defined by

$$\mathbf{u}^n = \sum_{i=1}^{n} \begin{bmatrix} f_1^i \, v_1^i \\ f_2^i \, v_2^i \\ f_3^i \, v_3^i \end{bmatrix} \tag{11}$$

The test functions are

$$\delta(\mathbf{f} \circ \mathbf{v}) = \delta\mathbf{f} \circ \mathbf{v} + \delta\mathbf{v} \circ \mathbf{f} \tag{12}$$

with

$$\mathbf{v} = \begin{bmatrix} v_1 \\ v_2 \\ v_3 \end{bmatrix} \quad \mathbf{f} = \begin{bmatrix} f_1 \\ f_2 \\ f_3 \end{bmatrix} \tag{13}$$

Introducing the test function defined by Eq. (12) and the trial function defined by Eq. (10) into the weak form Eq. (5), the two following equations to be solved can be deduced:

- for the test function $\delta\mathbf{f}$

$$a(\mathbf{v}\circ\mathbf{f},\mathbf{v}\circ\delta\mathbf{f}) = b(\mathbf{v}\circ\delta\mathbf{f}) - a(\mathbf{u}^n,\mathbf{v}\circ\delta\mathbf{f}) \quad \forall\delta\mathbf{f} \tag{14}$$

- for the test function $\delta\mathbf{v}$

$$a(\mathbf{f}\circ\mathbf{v},\mathbf{f}\circ\delta\mathbf{v}) = b(\mathbf{f}\circ\delta\mathbf{v}) - a(\mathbf{u}^n,\ \mathbf{f}\circ\delta\mathbf{v}) \quad \forall\delta\mathbf{v} \tag{15}$$

From Eq. (14) and Eq. (15), a coupled non-linear problem is derived. A fixed point method is a simple way to solve it. Starting from an initial function $(\tilde{\mathbf{f}}^{(0)},\tilde{\mathbf{v}}^{(0)})$, we construct a sequence $(\tilde{\mathbf{f}}^{(l)},\tilde{\mathbf{v}}^{(l)})$ which satisfy Eq. (14) and Eq. (15) respectively. Only 1D or 2D functions have to be found, as the other one is assumed to be known (from the previous step of the fixed point strategy). The fixed point algorithm is stopped when the distance between two consecutive terms are sufficiently small.

3.3. Finite element discretization

In this section, a classical finite element approximation in Ω and Ω_z for $(\mathbf{v},\mathbf{f})$ is introduced. The elementary vector of degrees of freedom (dof) associated with one element Ω_e of the mesh in Ω is denoted $\mathbf{q}_e^v$. The elementary vector of dofs associated with one element Ω_{ze} of the mesh in Ω_z is denoted $\mathbf{q}_e^f$. The displacement and strain fields are determined from the values of $\mathbf{q}_e^v$ and $\mathbf{q}_e^f$ by

$$\begin{aligned} \mathbf{v}_e &= \mathbf{N}_{xy}\mathbf{q}_e^v, \quad & \mathcal{E}_v^e &= \mathbf{B}_{xy}\mathbf{q}_e^v, \\ \mathbf{f}_e &= \mathbf{N}_z\mathbf{q}_e^f\ , \quad & \mathcal{E}_f^e &= \mathbf{B}_z\mathbf{q}_e^f \end{aligned} \tag{16}$$

where

$$\mathcal{E}_v^{eT} = \left[\begin{array}{cccccccccc} v_1 & v_{1,1} & v_{1,2} & v_2 & v_{2,1} & v_{2,2} & v_3 & v_{3,1} & v_{3,2} \end{array}\right]$$
$$\mathcal{E}_f^{eT} = \left[\begin{array}{cccccc} f_1 & f_1' & f_2 & f_2' & f_3 & f_3' \end{array}\right]$$

The matrices $\mathbf{N}_{xy}$, $\mathbf{B}_{xy}$, $\mathbf{N}_z$, $\mathbf{B}_z$ contain the interpolation functions, their derivatives and the jacobian components.

3.4. Finite element problem to be solved on Ω

For the sake of simplicity, the functions $\tilde{\mathbf{f}}^{(l)}$ which are assumed to be known, will be denoted $\tilde{\mathbf{f}}$. And the function $\tilde{\mathbf{v}}^{(l)}$ to be computed will be denoted $\mathbf{v}$. The strains included in Eq. (15) are defined as

$$\boldsymbol{\varepsilon}(\tilde{f} \circ v) = \boldsymbol{\Sigma}_{\mathbf{z}}(\tilde{f})\mathcal{E}_{\mathbf{v}} \tag{17}$$

with

$$\boldsymbol{\Sigma}_{\mathbf{z}}(\tilde{f}) = \begin{bmatrix} 0 & \tilde{f}_1 & 0 & 0 & 0 & 0 & 0 & 0 & 0 \\ 0 & 0 & 0 & 0 & 0 & \tilde{f}_2 & 0 & 0 & 0 \\ 0 & 0 & 0 & 0 & 0 & 0 & \tilde{f}_3' & 0 & 0 \\ 0 & 0 & 0 & \tilde{f}_2' & 0 & 0 & 0 & 0 & \tilde{f}_3 \\ \tilde{f}_1' & 0 & 0 & 0 & 0 & 0 & 0 & \tilde{f}_3 & 0 \\ 0 & 0 & \tilde{f}_1 & 0 & \tilde{f}_2 & 0 & 0 & 0 & 0 \end{bmatrix} \tag{18}$$

For convenience reasons, the displacement $\mathbf{u}$ is written under the form $\mathbf{u} = \mathbf{D}_{\mathbf{z}}(\tilde{f})\mathbf{v} = \begin{bmatrix} \tilde{f}_1 & 0 & 0 \\ 0 & \tilde{f}_2 & 0 \\ 0 & 0 & \tilde{f}_3 \end{bmatrix} \mathbf{v}$

The variational problem defined on Ω from Eq. (15) is

$$\int_{\Omega} \delta{\mathcal{E}_{\mathbf{v}}}^T \mathbf{k}_z(\tilde{f})\mathcal{E}_{\mathbf{v}} d\Omega = \int_{\partial\mathcal{V}_{F_{xy}}} \delta\mathbf{v}^T \mathbf{F}_z(\tilde{f})\, d\partial\mathcal{V} - \int_{\Omega} \delta{\mathcal{E}_{\mathbf{v}}}^T \sigma_{\mathbf{z}}(\tilde{f}, u^n) d\Omega \tag{19}$$

where

$$\begin{aligned} \mathbf{k}_z(\tilde{f}) &= \sum_{k=1}^{NC} \int_{\Omega_z^k} g^{(k)}(z)\ \boldsymbol{\Sigma}_{\mathbf{z}}(\tilde{f})^T \mathbf{C}_0^{(k)} \boldsymbol{\Sigma}_{\mathbf{z}}(\tilde{f}) dz \\ \sigma_{\mathbf{z}}(\tilde{f}, u^n) &= \sum_{k=1}^{NC} \int_{\Omega_z^k} g^{(k)}(z)\ \boldsymbol{\Sigma}_{\mathbf{z}}(\tilde{f})^T \mathbf{C}_0^{(k)} \boldsymbol{\varepsilon}(u^n) dz \\ \mathbf{F}_z(\tilde{f}) &= \mathbf{D}_{\mathbf{z}}(\tilde{f})^T \mathbf{t}\Big|_{z=z_F} \end{aligned} \tag{20}$$

The introduction of the finite element approximation Eq. (16) in the variational Eq. (19) leads to the linear problem:

$$\mathbf{K}_z(\tilde{f})\, \mathbf{q}^v = \mathbf{R}_{\mathbf{v}z}(\tilde{f},\ u^n) \tag{21}$$

where

- $\mathbf{q}^v$ is the vector of the nodal displacements, associated with the finite element mesh in Ω,
- $\mathbf{K}_z(\tilde{f})$ is the mechanical stiffness matrix obtained by summing the elements' stiffness matrices $\mathbf{K}_z^e(\tilde{f}) = \int_{\Omega_e} \left[\mathbf{B}_{xy}^T \mathbf{k}_z(\tilde{f}) \mathbf{B}_{xy}\right] d\Omega_e$
- $\mathbf{R}_{\mathbf{v}z}(\tilde{f}, u^n)$ is the equilibrium residual obtained by summing the elements' residual load vectors $\mathbf{R}_{\mathbf{v}z}^{\mathbf{e}}(\tilde{f}, u^n) = \int_{\partial \mathcal{V}_{F_{xy}}^e} \mathbf{N}_{xy}^T \mathbf{F}_z(\tilde{f}) d\partial\mathcal{V}_e - \int_{\Omega_e} \mathbf{B}_{xy}^T \sigma_{\mathbf{z}}(\tilde{f}, u^n) d\Omega_e$

3.5. Finite element problem to be solved on Ω_z

As in the previous section, the known functions $\tilde{\mathbf{v}}^{(l-1)}$ will be denoted $\tilde{\mathbf{v}}$ and the functions $\tilde{\mathbf{f}}^{(l)}$ to be computed will be denoted $\mathbf{f}$. The strain included in Eq. (14) is defined as

$$\boldsymbol{\varepsilon}(\tilde{v} \circ f) = \boldsymbol{\Sigma}_{\mathbf{xy}}(\tilde{v}) \mathcal{E}_{\mathbf{f}} \tag{22}$$

where

$$\boldsymbol{\Sigma}_{\mathbf{xy}}(\tilde{v}) = \begin{bmatrix} \tilde{v}_{1,1} & 0 & 0 & 0 & 0 & 0 \\ 0 & 0 & \tilde{v}_{2,2} & 0 & 0 & 0 \\ 0 & 0 & 0 & 0 & 0 & \tilde{v}_3 \\ 0 & 0 & 0 & \tilde{v}_2 & \tilde{v}_{3,2} & 0 \\ 0 & \tilde{v}_1 & 0 & 0 & \tilde{v}_{3,1} & 0 \\ \tilde{v}_{1,2} & 0 & \tilde{v}_{2,1} & 0 & 0 & 0 \end{bmatrix} \tag{23}$$

and the displacement is $\mathbf{u} = \mathbf{D}_{\mathbf{xy}}(\tilde{v}) \mathcal{E}_{\mathbf{f}} = \begin{bmatrix} \tilde{v}_1 & 0 & 0 & 0 & 0 & 0 \\ 0 & 0 & 0 & 0 & 0 & 0 \\ 0 & 0 & \tilde{v}_2 & 0 & 0 & 0 \\ 0 & 0 & 0 & 0 & 0 & 0 \\ 0 & 0 & 0 & 0 & \tilde{v}_3 & 0 \\ 0 & 0 & 0 & 0 & 0 & 0 \end{bmatrix} \mathcal{E}_{\mathbf{f}}$

The variational problem defined on Ω_z from Eq. (14) is

$$\sum_{k=1}^{NC} \int_{\Omega_z^k} g^{(k)}(z)\ \delta{\mathcal{E}_{\mathbf{f}}}^T \mathbf{k}_{xy}^{(k)}(\tilde{v}) \mathcal{E}_{\mathbf{f}} dz = \delta{\mathcal{E}_{\mathbf{f}}}^T\big|_{z=z_F}\ \mathbf{F}_{xy}(\tilde{v}) - \sum_{k=1}^{NC} \int_{\Omega_z^k} g^{(k)}(z)\ \delta{\mathcal{E}_{\mathbf{f}}}^T {\sigma_{\mathbf{xy}}}^{(k)}(\tilde{v}, u^n) dz \tag{24}$$

where $\mathbf{k}_{xy}^{(k)}(\tilde{v})$, ${\sigma_{\mathbf{xy}}}^{(k)}(\tilde{v}, u^n)$ and $\mathbf{F}_{xy}(\tilde{v})$ can be expressed under the following separated form:

$$\begin{aligned}
\mathbf{k}_{xy}^{(k)}(\tilde{v}) &= \int_{\Omega} \mathbf{\Sigma_{xy}}(\tilde{v})^T \mathbf{C}_0^{(k)} \mathbf{\Sigma_{xy}}(\tilde{v}) d\Omega \\
{\sigma_{\mathbf{xy}}}^{(k)}(\tilde{v}, u^n) &= \int_{\Omega} \mathbf{\Sigma_{xy}}(\tilde{v})^T \mathbf{C}_0^{(k)} \boldsymbol{\varepsilon}(u^n) d\Omega \\
\mathbf{F}_{xy}(\tilde{v}) &= \int_{\partial \mathcal{V}_{F_{xy}}} \mathbf{D_{xy}}(\tilde{v})^T \mathbf{t}\, d\partial\mathcal{V}_{xy}
\end{aligned} \tag{25}$$

Note that the computation of $\mathbf{k}_{xy}^{(k)}$ depends on the type of involved layers, i.e. FGM or classical layer.

The introduction of the finite element discretization Eq. (16) in the variational Eq. (24) leads to the linear problem:

$$\mathbf{K}_{xy}(\tilde{v})\, \mathbf{q}^f = \mathcal{R}_f(\tilde{v}, u^n) \tag{26}$$

where

- $\mathbf{q}^f$ is the vector of degree of freedom associated with the F.E. approximations in Ω_z.
- $\mathbf{K}_{xy}(\tilde{v})$ is obtained by summing the elements' stiffness matrices:

$${\mathbf{K}_{xy}}^e(\tilde{v}) = \int_{\Omega_{ze}^k} g^{(k)}(z)\ \Big[\mathbf{B}_z^T \mathbf{k}_{xy}^{(k)}(\tilde{v}) \mathbf{B}_z\Big] dz_e \tag{27}$$

- $\mathcal{R}_f(\tilde{v}, u^n)$ is obtained by summing the residual' vectors:

$$\mathcal{R}_f^e(\tilde{v}, u^n) = \mathbf{B}_z^T|_{z=z_F} \mathbf{F}_{xy}(\tilde{v}) - \int_{\Omega_{ze}^k} \Big[g^{(k)}(z)\ \mathbf{B}_z^T {\sigma_{\mathbf{xy}}}^{(k)}(\tilde{v}, u^n)\Big] dz_e \tag{28}$$

4. Numerical results

In the numerical examples, an eight-node quadrilateral FE based on the classical Serendipity interpolation functions is used for the unknowns depending on the in-plane coordinates. For the unknowns depending on the z-coordinate, the displacement is described by a fourth-order interpolation as it is justified in [39]. A Gaussian numerical integration with 3×3 points is used to evaluate the elementary matrices. As far as the integration with respect to the transverse coordinate is concerned, 5 integrations points are chosen in each numerical layer. The present approach, denoted VS-LD4, is compared with both reference solutions and other models available in open literature.

Hereafter, two classical numerical examples given by [20] are addressed to assess the accuracy of the present method. A one-layered plate and a sandwich structure are considered with different slenderness ratios and values of volume fraction exponent. Moreover, a third example from [41] is studied involving laminates with both FGM and orthotropic layers. Unless otherwise mentioned, the fourth-order layerwise model LD4, referring to the systematic work of Carrera ("Carrera's Unified Formulation" (CUF)) will be considered as the reference solution. This approach is based on a displacement formulation, and each displacement component is expanded until the fourth-order. $12NC + 3$ unknown functions are used in this kinematic.
Note that only one couple is built for each test due to the type of load and boundary conditions.

4.1. one-layered FGM plate

In this section, one-layered FGM plate is considered with different slenderness ratios. The data is given as follows:

geometry: square FGM plate with length-to-thickness ratio $S = a/h = 4, 10$

boundary conditions: simply-supported plate subjected to a bi-sinusoidal pressure: $p(x, y) = p_0 \sin(\frac{\pi x}{a}) \sin(\frac{\pi y}{b})$

material properties: elastic properties varying along the thickness direction z by a polynomial law, as proposed by Zenkour [6]; The plate is made of aluminum on the bottom and alumina on the top, and the following functional relationship is considered for $E(z)$:

$$E(z) = E_m + (E_c - E_m)\left(\frac{2z+h}{2h}\right)^k$$

where $E_m = 70$ GPa, $E_c = 380$ GPa are the elastic modulus of the aluminium and alumina, respectively. k is the volume fraction exponent ($k > 0$). $\nu = 0.3$ is considered as constant.

mesh: $N_x = N_y = 32$ where N_x and N_y are the number of elements along the x and y directions, respectively.

number of dofs: $Ndof_{xy} = 3.(3.N_x.N_y + 2(N_x + N_y) + 1)$ and $Ndof_z = 12.N_z + 3$ are the number of dofs of the two problems associated with v_j^i and f_j^i respectively. N_z is the number of numerical layers. So, the total number of dofs is $Ndof_{xy} + Ndof_z$.

results displacements and stresses are made non-dimensional according to

$$\bar{u}(z) = u_1(0, b/2, z)\ \frac{100\ E_c\ h^3}{p_0\ a^4};\ \bar{w}(z) = u_3(a/2, b/2, z)\ \frac{10\ E_c\ h^3}{p_0\ a^4};$$

$$\bar{\sigma}_{11}(z) = \sigma_{11}(a/2, b/2, z)\ \frac{h}{a\ p_0};\ \bar{\sigma}_{13}(z) = \sigma_{13}(0, b/2, z)\ \frac{h}{a\ p_0};\ \bar{\sigma}_{33}(z) = \sigma_{33}(a/2, b/2, z)$$

4.1.1. Convergence study

A convergence study is carried out for two values of k corresponding to two different distributions of properties through the thickness. In-plane and out-of-plane mesh refinements are considered independently. First, Tab. 1 shows the convergence of the displacements and stresses with a fixed value of $N_z = 4$. Classically, the convergence rate of the displacement is fast. Only $N_x = N_y = 4$ is sufficient. For stresses, 32 elements are needed to achieve convergence. We also notice that the in-plane mesh has to be rather fine so that the boundary conditions on the transverse normal stress be fulfilled and it seems to be more difficult for $k = 10$.

[Table 1 about here.]

Considering a mesh with $N_x = N_y = 32$ elements, the influence of the numerical layers is addressed in Tab. 2. For the displacements, the convergence rate is high as above. For the stresses, the influence of the value of k on the convergence rate is more pronounced. For $k = 10$, a higher Young modulus gradient through the thickness occurs and 8 numerical layers are needed. For $k = 1$, only 2 are sufficient. The transverse normal stress is the most sensitive value to the mesh.

[Table 2 about here.]

For further illustration, the distributions of $\bar{\sigma}_{13}$ and $\bar{\sigma}_{33}$ through the thickness are given in Fig. 2 for $k = 10$. It can be inferred from this figure that one numerical layer is insufficient to achieve accurate results. The boundary conditions are satisfied with at least 4 numerical layers.

[Figure 2 about here.]

4.1.2. Piecewise constant Young Modulus: Convergence study

As in [28] and [30], the FGM plate is modelized using a piecewise constant Young modulus. The influence of the number of numerical layers is studied hereafter. E is constant in each numerical layer, the value is taken at the middle of the layer. This type of computations can be performed in a commercial software considering numerous materials. Here, the PGD framework is advantageous as the computational cost is reduced even using high number of layers, as only 1D problems are involved (see [39]). To illustrate that, Tab. 3 gives the comparison between the present method (VS-LD4) vs the fourth-order LW expansion approach (LD4) in terms of the number of unkowns. The gain becomes very high when the number of layers increases. Thus, it is interesting to investigate this issue with the present numerical tool. For that, the error with respect to the mesh refinement is given in a log-log curve in Fig. 3 for both displacements and stresses. The convergence rate is the same for all the quantities excepted for the in-plane stress (divided by two). For this latter, numerical layers imply discontinuities between each element in the thickness direction, so high number

of numerical layers is required to circumvent this disadvantage. An illustration is shown in Fig. 4. It can be also noted that oscillations occurs even with $N_z = 64$ numerical layers.

[Table 3 about here.]

[Figure 3 about here.]

[Figure 4 about here.]

4.1.3. Different configurations for the one-layer test case

Based on the previous convergence studies, the subsequent computations are performed using a 32×32 mesh with 8 numerical layers. Note that the reference solution (LD4) involves also 8 numerical layers.

Two slenderness ratios (thick and semi-thick configurations) with two values of k are considered. Results are summarized in Tab. 4 and Tab. 5. Results are in excellent agreement with the LD4 model for both displacements and stresses, regardless the values of S and k. The error rate is less than 0.1%. As the LD4 model gives quasi-3D results, the present results are very satisfactory.

[Table 4 about here.]

[Table 5 about here.]

For further comparison, results of the present model are compared with other models (see Tab. 6) from open literature for different values of the volume fraction exponent k. The results are summarized in Tab. 7. The reference solution, denoted Q3D, is issued from [28]. For all models, the accuracy of the displacements is excellent. Nevertheless, when k increases, the HSDT model drives to an error rate of more than 8% for the transverse shear stress. Layerwise type models are required to compute accurate transverse stresses for all cases. Moreover, in [16], the authors have highlighted the importance to take into account the transverse stretching in the model. This phenomenon is included in the present approach.

[Table 6 about here.]

[Table 7 about here.]

The distributions of the in-plane and transverse shear stress through the thickness are also provided in Fig. 5 for $k = 1$ and $k = 10$. Results issued from the LD4 model are not given for clarity reason because the agreement with the present model is excellent. The satisfaction of the free boundary conditions is clear. We also notice the influence of the volume fraction exponent on the in-plane stress. A high stress gradient occurs on the top of the plate when k increases.
For this test case, the number of dofs of the LD4 model (316899 dofs) is 33 times greater than the VS-LD4 model.

[Figure 5 about here.]

4.2. Sandwich plate

In this section, a sandwich plate is considered. The test case is described as follows:

geometry: square sandwich plate ($a = b = 1$ m) with length-to-thickness ratio $S = 4, 20$, constituted of three layers, the thickness of the faces and the core is $h_f = 0.1h$ and $h_c = 0.8h$, respectively.

boundary conditions: simply-supported plate on all sides subjected to a bi-sinusoidal pressure $p(x, y) = p_0 \sin \dfrac{\pi x}{a} \sin \dfrac{\pi y}{b}$

material properties: The two external faces are in aluminium at the bottom and in alumina at the top.
bottom face sheets: isotropic material with $E = 70$ GPa, $\nu = 0.3$ (aluminium)
top face sheets: isotropic material with $E = 380$ GPa, $\nu = 0.3$ (alumina)
Core : FGM as in Section 4.1

mesh: $N_x = N_y = 32$

number of dofs: $Ndof_{xy} = 9603$ and $Ndof_z = 12.N_z + 3 = 111$

number of dofs for LD4: $N_{LW} = 3.(4.N_z + 1).(3.N_x.N_y + 2(N_x + N_y) + 1) = 355311$

results: non-dimensional results as in Section 4.1

First of all, the importance of the numerical layers is highlighted to compute the transverse stresses. As illustrated in Fig. 6, a high discontinuity occurs at the interface between the core and the upper face when using one numerical layer per physical layer. It can be circumvented by introducing three numerical layers.
In the subsequent example, the results are given following this recommandation.

[Figure 6 about here.]

Different slenderness ratios and values of k are considered to assess the accuracy of the method. The results are summarized in Tab. 8. For both thin and thick cases, whatever the values of the volume fraction exponent, the results are in excellent agreement with the reference solution. The distribution of the in-plane and transverse shear stresses are also given in Fig. 7 for $k = 1$ and $k = 10$. The complex distribution of $\bar{\sigma}_{11}$ through the thickness is well represented. The traction free condition is fulfilled on the top and bottom surfaces.

[Table 8 about here.]

[Figure 7 about here.]

4.3. Multilayered FGM plate

In this section, the static behavior of a multilayered FGM plate is studied. The test case given in [41] is such as

geometry: square sandwich plate ($a = b = 1$ m) with length-to-thickness ratio $S = 5$, constituted of three layers $[FGM/0°/FGM]$, the thickness of the 3 layers are the same.

boundary conditions: simply-supported plate on all sides subjected to a bi-sinusoidal pressure $p(x,y) = p_0 \sin\dfrac{\pi x}{a} \sin\dfrac{\pi y}{b}$

material properties: $\begin{array}{rcl} E_L & = & 25\,\text{GPa}\ ,\ E_T = 1\,\text{GPa}\ ,\ G_{LT} = 0.2\,\text{GPa}\ , \\ G_{TT} & = & 0.5\,\text{GPa}\ ,\ \nu_{LT} = \nu_{TT} = 0.25 \end{array}$ where L refers to the fiber direction, T refers to the transverse direction.

The FGM material is such that :

$g^{(1)}(z) = \exp(k_{exp}\frac{z+h/6}{-h/3})$ for $-h/2 \leq z \leq -h/6$

$g^{(3)}(z) = \exp(k_{exp}\frac{z-h/6}{h/3})$ for $h/6 \leq z \leq h/2$

with the material-property gradient index: $k_{exp} = 5$

mesh: $N_x = N_y = 32$

results: The results are made nondimensional using:

$\bar{u} = u_1(0, b/2, z)\dfrac{E_T}{hq_0S^3}$, $\bar{\sigma}_{\alpha\alpha} = \dfrac{\sigma_{\alpha\alpha}(a/2, b/2, z)}{q_0S^2}$

$\bar{\sigma}_{13} = \dfrac{\sigma_{13}(0, b/2, z)}{q_0S}$, $\bar{\sigma}_{33} = \dfrac{\sigma_{33}(a/2, b/2, z)}{q_0}$

reference values exact elasticity results are given in [41] and obtained from [42].

This example seems to be a severe test case. The results will be compared with two Third-order Shear Deformation Theories with a displacement-based (denoted TSDT-Wu) and a RMVT-based (denoted RMVT-Wu) approach available in [41]. Note that the transverse normal strain is assumed to be nil in these works. For the present approach, three numerical layers per physical layer is required to improve the accuracy of the transverse shear and normal stresses. The in-plane displacement and stress, and the transverse shear / normal stresses are shown in Fig. 8 and Fig. 9. It can be inferred from these figures that the VS-LD4 method is in excellent agreement with the exact solution. The RMVT approach is not sufficient to recover accurate results. Indeed, as previously observed in open literature, the influence of the stretching effect is of major importance.

[Figure 8 about here.]

[Figure 9 about here.]

5. Conclusion

In this article, an approach based on a variable separation method has been extended to model FGM plates. The results are assessed with various representative benchmarks by comparing with both reference solutions and results issued from other theories. It can be concluded that the present approach drives to very accurate results regardless of the type of configurations with one-layered FGM, sandwich or mixed classical/FGM layers. It has also been shown that numerical layers are needed to compute the transverse shear and normal stresses with accuracy. Another possibility of the method is illustrated through the consideration of piecewise constant mechanical properties to model such structures. The advantage of the method in terms of computational cost comparing with Layerwise or 3D model is highlighted.

References

[1] M. Naebe, K. Shirvanimoghaddam, Functionally graded materials: A review of fabrication and properties, Applied Materials Today 5 (2016) 223–245.

[2] R. Parihar, S. Setti, R. Sahu, Recent advances in the manufacturing processes of functionally graded materials: a review, Science and Engineering of Composite Materials 25 (2) (2018) 309–336.

[3] V. Birman, L. W. Byrd, Modeling and analysis of functionally graded materials and structures., Appl. Mech. Rev. 60 (5) (2007) 195–216.

[4] A. Gupta, M. Talha, Recent development in modeling and analysis of functionally graded materials and structures., Progress in Aerospace Sciences 79 (2015) 1–14.

[5] M. Kashtalyan, Three-dimensional elasticity solution for bending of functionally graded rectangular plates., European J. of Mechanics A. Solids 23 (2004) 853–64.

[6] M. Kashtalyan, M. Menshykova, Three-dimensional elasticity solution for sandwich panels with a functionally graded core., Compos. Struct. 87 (2008) 36–43.

[7] V. Burlayenko, T. Sadowski, Free vibrations and static analysis of functionally graded sandwich plates with three-dimensional finite elements, Meccanica 55 (4) (2020) 815–832.

[8] S.-H. Chi, Y.-L. Chung, Mechanical behavior of functionally graded material plates under transverse load - part i: Analysis., Int. J. Solids Struct. 43 (13) (2006) 3657–3674.

[9] Z. Cheng, R. Batra, Deflection relationships between the homogeneous kirchhoff plate theory and different functionally graded plate theories, Archives of Mechanics 52 (1) (2000) 143–158.

[10] J. Reddy, Analysis of functionally graded plates., Int. J. Num. Meth. Eng. 47 (2000) 663–684.

[11] A. Ferreira, R. Batra, C. Roque, L. Qian, P. Martins, Static analysis of functionally graded plates using third-order shear deformation theory and a meshless method, Compos. Struct. 69 (4) (2005) 449–457.

[12] R. Kumar, A. Lal, B. Singh, J. Singh, New transverse shear deformation theory for bending analysis of FGM plate under patch load., Compos. Struct. 208 (2019) 91–100.

[13] V.-H. Nguyen, T.-K. Nguyen, H.-T. Thai, T. Vo, A new inverse trigonometric shear deformation theory for isotropic and functionally graded sandwich plates, Composite Part B : Eng. J. 66 (2014) 233–246.

[14] H. Nguyen-Xuan, L. V. Tran, C. H. Thai, S. Kulasegaram, S. Bordas, Isogeometric analysis of functionally graded plates using a refined plate theory., Composite Part B : Eng. J. 64 (2014) 222–234.

[15] M. Li, C. G. Soares, R. Yan, A novel shear deformation theory for static analysis of functionally graded plates., Compos. Struct. 250 (2020) 112559.

[16] E. Carrera, S. Brischetto, M. Cinefra, M. Soave, Effects of thickness stretching in functionally graded plates and shells., Composite Part B : Eng. J. 42 (2011) –.

[17] L. Qian, R. Batra, L. Chen, Static and dynamic deformations of thick functionally graded elastic plates by using higher-order shear and normal deformable plate theory and meshless local petrov–galerkin method, Composite Part B : Eng. J. 35 (6-8) (2004) 685–697.

[18] S. Natarajan, M. Ganapathi, Bending and vibration of functionally graded material sandwich plates using an accurate theory., Finite Elem. Anal. Des. 57 (2012) 32–42.

[19] H.-T. Thai, D.-H. Choi, Improved refined plate theory accounting for effect of thickness stretching in functionally graded plates, Composite Part B : Eng. J. 56 (2014) 705–716.

[20] A. Zenkour, Generalized shear deformation theory for bending analysis of functionally graded plates., Appl. Math. Model. 30 (2006) 67–84.

[21] A. Neves, A. Ferreira, E. Carrera, C. Roque, M. Cinefra, R. Jorge, C. Soares, A quasi-3d sinusoidal shear deformation theory for the static and free vibration analysis of functionally graded plates., Composite Part B : Eng. J. 43 (2012) 711–725.

[22] J. Mantari, C. G. Soares, Generalized hybrid quasi-3d shear deformation theory for the static analysis of advanced composite plates., Compos. Struct. 94 (8) (2012) 2561–2575.

[23] J. Mantari, C. G. Soares, Optimized sinusoidal higher order shear deformation theory for the analysis of functionally graded plates and shells, Composite Part B : Eng. J. 56 (2014) 126–136.

[24] H.-T. Thai, S.-E. Kim, A simple quasi-3d sinusoidal shear deformation theory for functionally graded plates., Compos. Struct. 99 (2013) 172–180.

[25] J. Mantari, C. G. Soares, Five-unknowns generalized hybrid-type quasi-3d hsdt for advanced composite plates, Appl. Math. Model. 39 (18) (2015) 5598–5615.

[26] Z. Belabed, M. Houari, A. Tounsi, S. Mahmoud, O. Bég, An efficient and simple higher order shear and

normal deformation theory for functionally graded material (FGM) plates, Composite Part B : Eng. J. 60 (2014) 274–283.

[27] J. Mantari, C. G. Soares, Four-unknown quasi-3d shear deformation theory for advanced composite plates, Compos. Struct. 109 (2014) 231–239.

[28] E. Carrera, S. Brischetto, A. Robaldo, Variable kinematic model for the analysis of functionally graded material plates., AIAA J. 46 (2008) 194–203.

[29] S. Brischetto, E. Carrera, Advanced mixed theories for bending analysis of functionally graded plates., Comput. Struct. 88 (2010) 1474–1483.

[30] F. Ramirez, P. Heyliger, E. Pan, Static analysis of functionally graded elastic anisotropic plates using a discrete layer approach, Composites Part B: Engineering 37 (1) (2006) 10–20.

[31] D. Jha, T. Kant, R. Singh, A critical review of recent research on functionally graded plates, Compos. Struct. 96 (2013) 833–849. doi:https://doi.org/10.1016/j.compstruct.2012.09.001.

[32] K. Swaminathan, D. Naveenkumar, A. Zenkour, E. Carrera, Stress, vibration and buckling analyses of FGM plates - a state-of-the-art review., Compos. Struct. 120 (2015) 10–31.

[33] H.-T. Thai, S.-E. Kim, A review of theories for the modeling and analysis of functionally graded plates and shells, Compos. Struct. 128 (2015) 70–86.

[34] P. S. Ghatage, V. R. Kar, P. E. Sudhagar, On the numerical modelling and analysis of multi-directional functionally graded composite structures: A review, Compos. Struct. 236 (2020) 111837. doi:https://doi.org/10.1016/j.compstruct.2019.111837.

[35] M. Aghdam, K. Bigdeli, N. Shahmansouri, A semi-analytical solution for bending of moderately thick doubly curved functionally graded panels, Mech. Advanced Mater. Struct. 17 (5) (2010) 320–327.

[36] M. Savoia, J. Reddy, A variational approach to three-dimensional elasticity solutions of laminated composite plates, J. Applied Mech. ASME 59 (1992) 166–175.

[37] B. Bognet, F. Bordeu, F. Chinesta, A. Leygue, A. Poitou, Advanced simulation of models defined in plate geometries: 3D solutions with 2D computational complexity., Comput. Methods Appl. Mech. Eng. 201-204 (2012) 1–12, doi: 10.1016/j.cma.2011.08.025.

[38] P. Vidal, L. Gallimard, O. Polit, Composite beam finite element based on the proper generalized decomposition., Comput. Struct. 102-103 (2012) 76–86, -doi: 10.1016/j.compstruc.2012.03.008.

[39] P. Vidal, L. Gallimard, O. Polit, Proper generalized decomposition and layer-wise approach for the modeling of composite plate structures., Int. J. Solids Struct. 50 (14-15) (2013) 2239–2250, -doi: 10.1016/j.ijsolstr.2013.03.034.

[40] J. Mantari, A. Oktem, C. G. Soares, A new trigonometric layerwise shear deformation theory for the finite element analysis of laminated composite and sandwich plates., Comput. Struct. 94-95 (2012) 45–53.

[41] C.-P. Wu, H.-Y. Li, An rmvt-based third-order shear deformation theory of multilayered functionally graded material plates, Compos. Struct. 92 (10) (2010) 2591–2605.

[42] C.-P. Wu, S.-J. Chen, K.-H. Chiu, Three-dimensional static behavior of functionally graded magneto-electro-elastic plates using the modified pagano method, Mech. Res. Commun. 37 (1) (2010) 54–60.

List of Figures

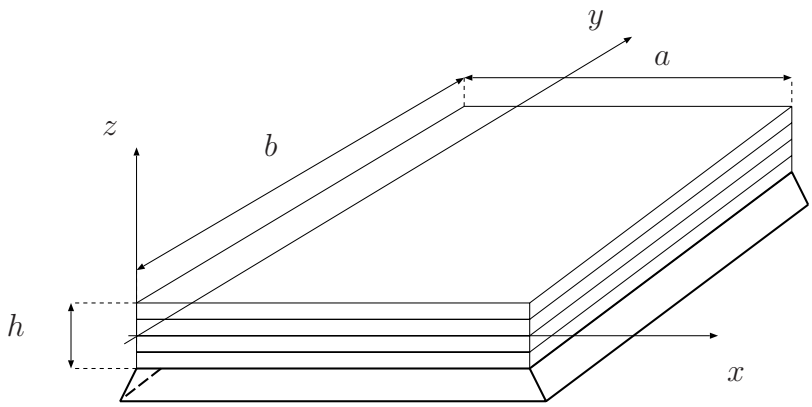

Figure 1: Geometry of the plate

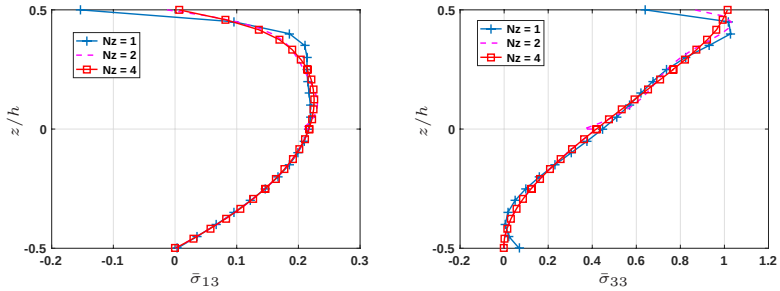

Figure 2: distribution of $\bar{\sigma}_{13}$ (left) and $\bar{\sigma}_{33}$ (right) along the thickness - S=10 - one-layered - polynomial law - $k = 10$

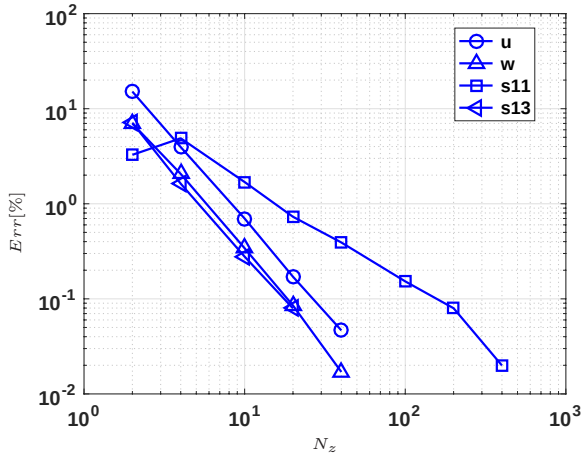

Figure 3: Convergence study - S=10 - one-layered - polynomial law - $k = 1$

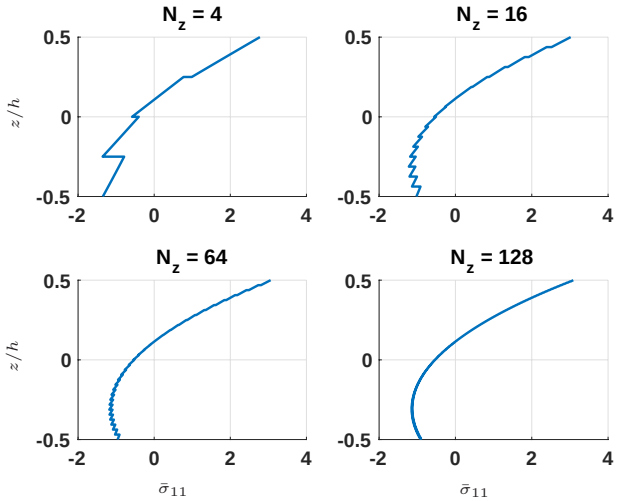

Figure 4: Distribution of the in-plane stress $\bar{\sigma}_{11}$ through the thickness for different values of numerical layers - S=10 - one-layered - polynomial law - piecewise constant Young Modulus - $k = 1$

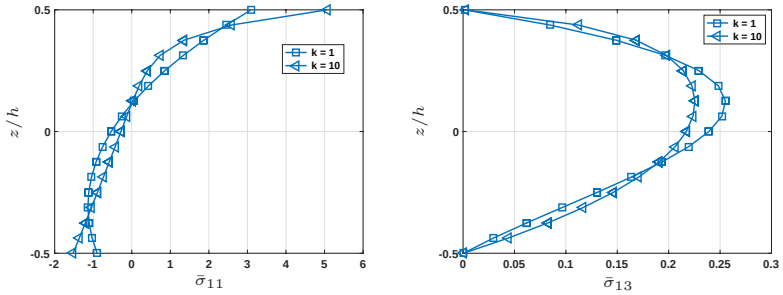

Figure 5: distribution of $\bar{\sigma}_{11}$ (left) and $\bar{\sigma}_{13}$ (right) along the thickness - S=10 - one-layered - polynomial law - $k = 1, 10$

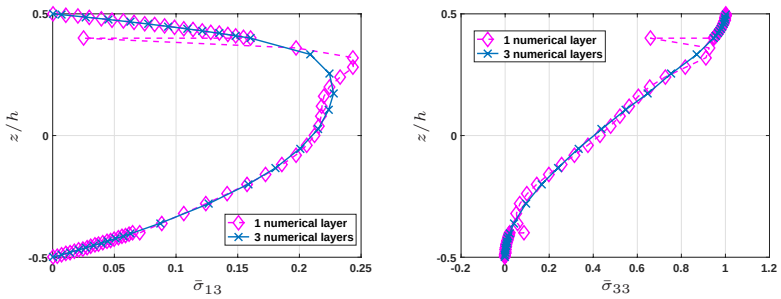

Figure 6: distribution of $\bar{\sigma}_{13}$ (left) and $\bar{\sigma}_{33}$ (right) along the thickness - S=4 - sandwich - polynomial law - $k = 10$

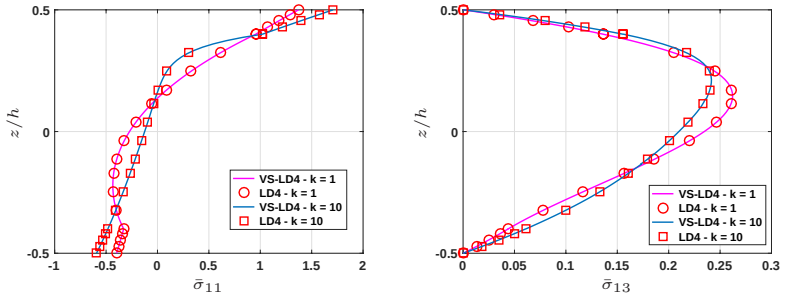

Figure 7: distribution of $\bar{\sigma}_{11}$ (left) and $\bar{\sigma}_{13}$ (right) along the thickness - S=4 - sandwich - polynomial law - $k = 1/10$

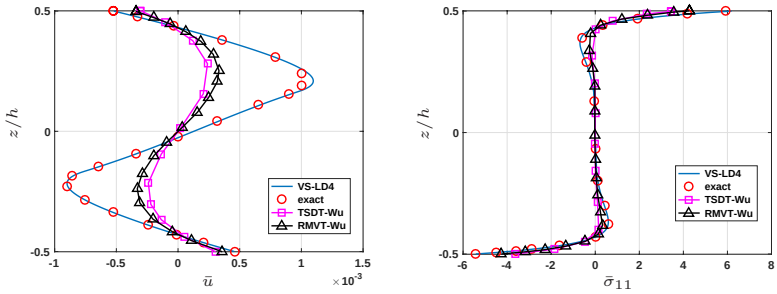

Figure 8: distribution of $\bar{u}$ (left) and $\bar{\sigma}_{11}$ (right) along the thickness - S=5 - 3-layer - exponential law

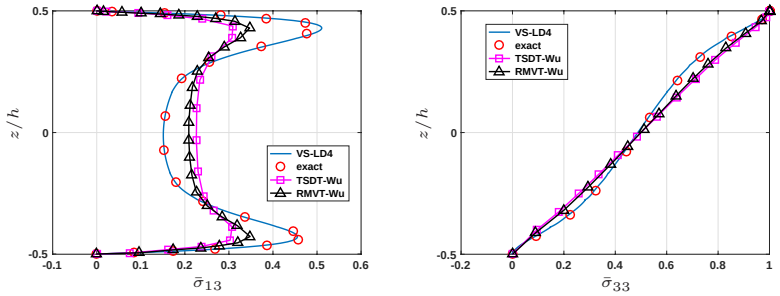

Figure 9: distribution of $\bar{\sigma}_{13}$ (left) and $\bar{\sigma}_{33}$ (right) along the thickness - S=5 - 3-layer - exponential law

List of Tables

k	$N_x = N_y$	$\bar{u}(-h/4)$	$\bar{w}(0)$	$\bar{\sigma}_{11}(h/3)$	$\bar{\sigma}_{33}(h/2)$	$\bar{\sigma}_{13}(h/6)$
1	1	0.5790	0.4478	1.2655	2.3411	0.8612
	2	0.6461	0.5798	1.5361	1.6133	0.4561
	4	0.6438	0.5870	1.5256	1.2594	0.3123
	8	0.6436	0.5875	1.5121	1.0753	0.2672
	16	0.6436	0.5875	1.5077	1.0196	0.2550
	32	0.6436	0.5875	1.5066	1.0049	0.2519
	64	0.6436	0.5875	1.5063	1.0012	0.2511
10	1	1.0066	0.8069	0.8090	4.1083	0.5376
	2	1.0874	0.9967	0.9205	2.2401	0.3270
	4	1.0844	1.0067	0.9069	1.4554	0.2531
	8	1.0842	1.0074	0.8983	1.1313	0.2313
	16	1.0842	1.0074	0.8957	1.0381	0.2256
	32	1.0842	1.0074	0.8950	1.0140	0.2241
	64	1.0842	1.0074	0.8948	1.0079	0.2238

Table 1: one-layered FGM plate - polynomial law - $b = a$ - $S = 10$ - $N_z = 4$

k	N_z	$\bar{u}(-h/4)$	$\bar{w}(0)$	$\bar{\sigma}_{11}(h/3)$	$\bar{\sigma}_{33}(h/2)$	$\bar{\sigma}_{13}(h/6)$
	1	0.6435	0.5875	1.5068	0.9892	0.2520
1	2	0.6436	0.5875	1.5066	1.0049	0.2519
	4	0.6436	0.5875	1.5066	1.0049	0.2519
	8	0.6436	0.5875	1.5066	1.0049	0.2519
	1	1.0848	1.0083	0.8977	0.6395	0.2165
10	2	1.0842	1.0074	0.8946	0.8643	0.2252
	4	1.0842	1.0074	0.8950	1.0140	0.2241
	8	1.0842	1.0074	0.8950	1.0092	0.2242

Table 2: one-layered FGM plate - polynomial law - $b = a$ - $S = 10$ - $N_x = N_y = 32$

N_z	4	16	64	128
N_{dof} VS-LD4	9654	9798	10374	11142
N_{dof} 4th order LW	163251	624195	2467971	4926339
N_{dof} 4th order LW / N_{dof} VS-LD4	17	64	238	442

Table 3: Comparison in terms of number of dofs between the present approach and the LW approach with a fourth-order expansion

S	Model	$\bar{u}(-h/4)$	$\bar{v}(-h/6)$	$\bar{w}(0)$	$\bar{\sigma}_{11}(h/3)$	$\bar{\sigma}_{33}(h/2)$	$\bar{\sigma}_{13}(h/6)$	$\bar{\sigma}_{23}(h/6)$
	VS-LD4	1.5967	1.2584	0.7172	0.6218	1.0009	0.2517	0.2517
4	LD4	1.5967	1.2584	0.7172	0.6218	1.0004	0.2517	0.2517
	Err	0.00	0.00	0.00	0.00	0.04	0.00	0.00
	VS-LD4	0.6436	0.4982	0.5875	1.5066	1.0049	0.2519	0.2519
10	LD4	0.6436	0.4982	0.5875	1.5066	1.0007	0.2519	0.2519
	Err	0.00	0.00	0.00	0.00	0.43	0.00	0.00

Table 4: one-layered FGM plate - polynomial law - $b = a$ - $N_x = N_y = 32$ - $k = 1$

S	Model	$\bar{u}(-h/4)$	$\bar{v}(-h/6)$	$\bar{w}(0)$	$\bar{\sigma}_{11}(h/3)$	$\bar{\sigma}_{33}(h/2)$	$\bar{\sigma}_{13}(h/6)$	$\bar{\sigma}_{23}(h/6)$
	VS-LD4	2.6857	2.1058	1.3756	0.3651	1.0072	0.2218	0.2218
4	LD4	2.6857	2.1058	1.3756	0.3651	1.0064	0.2218	0.2218
	Err	0.00	0.00	0.00	0.00	0.08	0.00	0.00
	VS-LD4	1.0842	0.8405	1.0074	0.8950	1.0140	0.2241	0.2241
10	LD4	1.0842	0.8405	1.0074	0.8950	1.0066	0.2241	0.2241
	Err	0.00	0.00	0.00	0.00	0.73	0.00	0.00

Table 5: one-layered FGM plate - polynomial law - $b = a$ - $N_x = N_y = 32$ - $k = 10$

Zenkour06 [20]	it refers to Generalized shear deformation theory. An ESL model including a sinus function with 5 unknowns is used. The transverse displacement is constant through the thickness. It satisfies the zero tangential traction boundary conditions on the surfaces of the plate. A Navier type solution is developed.
Mantari12 [40]	a High-order Shear Deformation Theory (HSDT) model is used with 5 generalized unknowns (ESL model). The tangential stress-free boundary conditions on the plate surfaces is satisfied. A Navier-type solution is carried out.

Table 6: models available in open literature

k	Model	$\bar{u}(-h/4)$	$\bar{v}(-h/6)$	$\bar{w}(0)$	$\bar{\sigma}_{11}(h/3)$	$\bar{\sigma}_{33}(h/2)$	$\bar{\sigma}_{13}(h/6)$	$\bar{\sigma}_{23}(h/6)$
	VS-LD4	0.6436	0.4982	0.5875	1.5066	1.0049	0.2519	0.2519
	Err VS-LD4	-	-	0.01	0.02	0.49	0.36	0.36
	LD4	0.6436	0.4982	0.5875	1.5066	1.0007	0.2519	0.2519
	Err-LD4	-	-	0.01	0.02	0.07	0.36	0.36
1	Zenkour06	-	-	0.5889	1.4894	1.0000	0.2622	0.2622
	Err-Zenkour06	-	-	0.24	1.12	0.00	4.46	4.46
	Mantari12	-	-	0.5880	1.4888	1.0000	0.2566	0.2566
	Err-Mantari12	-	-	0.09	1.16	0.00	2.23	2.23
	Q3D	-	-	0.5875	1.5062	1.0000	0.2510	0.2510
	VS-LD4	1.0541	0.8418	0.8823	1.1945	1.0071	0.2370	0.2370
	Err VS-LD4	-	-	0.00	0.33	0.71	0.32	0.32
	LD4	1.0541	0.8418	0.8823	1.1945	1.0013	0.2370	0.2370
	Err LD4	-	-	0.00	0.33	0.13	0.33	0.33
4	Zenkour06	-	-	0.8819	1.1783	1.0000	0.2580	0.2580
	Err-Zenkour06	-	-	0.05	1.69	0.00	9.23	9.23
	Mantari12	-	-	0.8814	1.1755	1.0000	0.2623	0.2623
	Err-Mantari12	-	-	0.10	1.92	0.00	11.05	11.05
	Q3D	-	-	0.8823	1.1985	1.0000	0.2362	0.2362
	VS-LD4	1.0842	0.8405	1.0074	0.8950	1.0140	0.2241	0.2241
	Err VS-LD4	-	-	0.00	0.66	1.40	0.19	0.19
	LD4	1.0842	0.8405	1.0074	0.8950	1.0066	0.2241	0.2241
10	Err-LD4	-	-	0.00	0.66	0.66	0.19	0.19
	Zenkour06 [20]	-	-	1.0089	0.8775	1.0000	0.2041	0.2041
	Err-Zenkour06	-	-	0.15	2.60	0.00	8.76	8.76
	Q3D	-	-	1.0074	0.9009	1.0000	0.2237	0.2237

Table 7: one-layered FGM plate - polynomial law - $b = a$ - $N_x = N_y = 32$ - $S = 10$

S	k	Model	$\bar{u}(-h/4)$	$\bar{v}(-h/6)$	$\bar{w}(0)$	$\bar{\sigma}_{11}(h/3)$	$\bar{\sigma}_{33}(h/2)$	$\bar{\sigma}_{13}(h/6)$	$\bar{\sigma}_{23}(h/6)$
		VS-LD4	1.8208	1.4565	0.7629	0.6532	1.0008	0.2615	0.2615
	1	LD4	1.8208	1.4565	0.7629	0.6532	1.0001	0.2615	0.2615
		Err	0.00	0.00	0.00	0.00	0.08	0.00	0.00
		VS-LD4	2.5596	2.1328	1.0934	0.5033	1.0010	0.2397	0.2397
4	4	LD4	2.5596	2.1328	1.0934	0.5033	1.0001	0.2397	0.2397
		Err	0.00	0.00	0.00	0.00	0.09	0.00	0.00
		VS-LD4	2.6353	2.1418	1.2239	0.3559	1.0010	0.2276	0.2276
	10	LD4	2.6353	2.1418	1.2239	0.3559	1.0001	0.2276	0.2276
		Err	0.00	0.00	0.00	0.00	0.09	0.00	0.00
		VS-LD4	0.3675	0.2882	0.6134	3.1619	1.0200	0.2648	0.2648
	1	LD4	0.3675	0.2882	0.6134	3.1618	1.0070	0.2649	0.2649
		Err	0.00	0.00	0.00	0.00	1.	0.01	0.01
		VS-LD4	0.5263	0.4249	0.7922	2.5531	1.0226	0.2425	0.2425
20	4	LD4	0.5263	0.4249	0.7922	2.5530	1.0090	0.2426	0.2426
		Err	0.00	0.00	0.00	0.00	1.	0.01	0.01
		VS-LD4	0.5367	0.4313	0.8242	1.9058	1.0239	0.2324	0.2324
	10	LD4	0.5367	0.4313	0.8242	1.9058	1.0095	0.2325	0.2325
		Err	0.00	0.00	0.00	0.00	1.	0.01	0.01

Table 8: sandwich FGM plate - polynomial law - $b = a$ - $N_x = N_y = 32$ - $S = 4/20$